Interdisciplinary Studies on Applied Science, 3 (1) :49–65, 2026. DOI: 10.58613/isas315

Interdisciplinary Studies on Applied Science

Journal homepage: https://www.gpub.org/journal-details.php?journal-id=42

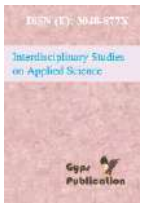

Research Article

Design, Synthesis and In Silico Evaluation of Benzotriazole-Based Urea Derivatives as Potential VEGFR-2 Inhibitors

Mohammed Zuheir Hassan [1*]

[1]*Department of Aesthetic and Laser Techniques, College of Health and Medical Technology, University of Alkafeel, Najaf, Iraq.*

[*]*Corresponding author Email: mohammed.zuheir@alkafeel.edu.iq*

Article Info

Keywords: *VEGFR-2 inhibition, Molecular docking, Structure activity relationship (SAR), ADMET, Angiogenesis inhibition, Tyrosine kinase inhibitors.*

Received: *10.03.2026;*

Accepted: *05.04.2026;*

Published: *12.04.2026;*

Abstract:

Vascular endothelial growth factor receptor-2 (VEGFR-2) is pivotal in the process of tumor angiogenesis and is a validated target for therapeutic intervention in cancer. Here, in this study reported the design, synthesis, and evaluation of a new series of benzotriazole-based urea derivatives (bc1–bc5) as potential VEGFR-2 inhibitors. The synthetic approach involved the N1-acylation of benzotriazole, followed by hydrazide formation and further reactions with a variety of substituted aromatic isocyanates to yield target compounds in good yields (69–78%). The structures of the synthesized derivatives were confirmed by FTIR, ^{1}H NMR, ^{13}C NMR, mass spectrometry, and elemental analysis. Molecular docking studies were performed against the VEGFR-2 kinase domain (PDB ID: 4ASD), using Sorafenib as the reference inhibitor. All compounds exhibited favorable binding affinities (−8.77 to −9.37 kcal/mol), with bc2 showing the highest docking score for the synthesized derivatives. The binding interactions showed critical hydrogen bonds with residues like CYS919 and ASP1046, along with a significant hydrophobic component and π–π interactions in the ATP-binding pocket. SAR analysis underlined the importance of the benzotriazole–urea scaffold and indicated that electron-withdrawing groups, especially CF_3, increased binding affinity. ADMET predictions showed good oral absorption, moderate distribution, acceptable physicochemical properties, and adherence to Lipinski's rule of five. However, CYP inhibition, hepatotoxicity, AMES positivity predicted that biological and toxicity evaluation should be carried out. Overall, this study demonstrates that the synthesized benzotriazole-based urea derivatives could represent useful lead candidates for continued development as anti-cancer agents targeting VEGFR-2.

1. Introduction

The WHO report of 2018 reveals that worldwide number of cancers could attain 22 million by 2030 [1, 2]. Therefore, making continuous effort to find and develop drugs with low toxicity and high potency is indispensable for progressing research in the anti-cancer drugs [3]. As tumors require blood vessels located around them for growth and metastasis, this phenomenon has been taken into consideration to inhibit angiogenesis as a strategy to rein in tumor spread [4-8]. Studies have found that vascular endothelial growth factor (VEGF), a growth factor acting on vascular endothelium, promotes the formation of blood vessels by stimulating both proliferation and motility of endothelial cells [6, 9-11]. The three main VEGF receptors, VEGFR-1, VEGFR-2, and VEGFR-3 are essential mediators of the angiogenic process that initiates a network of blood vessels that feeds the tumor with nutrients and oxygen [12-14]. VEGFR-2 is the predominant VEGF receptor and is critical for regulating the development of blood vessels [15-18]. It has been found that aberrant expression of VEGFR-2 in tumor cells lead them to spread and progress rapidly. Thus, inhibition targeting the VEGF/VEGFR-2 signaling pathway is a relevant mechanism for the generation of novel cancer therapeutic approaches [19]. Several small-molecules recently have been approved on the market to address this serious angiogenic avenue Pazopanib, Sorafenib, Sunitinib, Vandetanib, Axitinib [20]. Yet, the pursuit for new anti-angiogenic inhibitors is clearly warranted to avoid drug resistance. Heterocyclic compounds containing a benzene ring (not fully fused) and an azole ring are known as benzo-fused azoles [21, 22]. The azole ring usually features one or more nitrogen atoms. Benzotriazole is an example of a benzo-fused azole with three nitrogen atoms [23]. Benzotriazole and its derivatives exhibit various biological activities including antifungal and antibacterial [24, 25], anti-proliferative [26], anti-cancer [27], and antidiabetic [28] properties. In medicinal chemistry, benzotriazoles have found numerous applications, as reflected in the examples of Alizapride and Varazole [29, 30]. Conventional drug design techniques tend to be expensive, slow and require a laborious and cumbersome process owing to the need to proceed through all the stages from identification of the host to regulatory approval [31, 32]. The pre-bolus step of the traditional drug development approaches being time and cumbersome renders the promising candidates less likely to cross the finish line in faculties staging clinical trials. The result - the success rate plummeted from 34% over the period from 2011-2015 to 20% from 2016 to 2020 [33]. This steep drop in landslide success rates has resulted in the pharmaceutics looking for more compelling methods. As a result, scientists are looking to in silico approaches to consummate drug design. This shift in tactic is designed to reduce costs and time involved in arrays, and raises the odds of success and speeding times robotic slims of fresh medicinal products into the clinic [34, 35]. Utilizing computer algorithms and simulations, drug development methods have been expedited, enabling quicker discovery and improved optimization of new molecules Improvements in bioinformatics and better software have made progress in this area cheaper. Computational advances have facilitated drug developers by improving the realism of molecular modeling and drug efficacy prediction, speeding up the process, and increasing the probability of identifying possible drug candidates [36, 37].

2. Experimental Part

All reagents and solvents used were of analytical grade unless otherwise stated, and were used as received without further purification. Benzotriazole, chloroacetyl chloride, hydrazine hydrate, substituted aromatic isocyanates, triethylamine, dichloromethane (DCM), dimethylformamide (DMF), ethyl acetate, hexane, and ethanol were purchased from commercial suppliers. Reactions were typically monitored by thin-layer chromatography (TLC) using silica gel 60 F254 plates and visualised under UV light. Melting points were determined in open capillary

tubes and are uncorrected. FTIR spectra were recorded using KBr pellets and expressed in cm^{-1}. The department or division hosts a very active NMR community. The ^{1}H and ^{13}C NMR spectra were recorded at 400 MHz, with DMSO-d_6 as the solvent and tetramethylsilane (TMS) as the internal standard. Chemical shifts were reported in ppm (parts per million). The mass spectra were obtained by electron ionization (EI), and elemental analyses were performed to determine the elemental composition of the compounds.

2.1 Synthesis of 1-(Chloroacetyl) benzotriazole (a)

Benzotriazole (1 equiv.) was dissolved in dry dichloromethane and stirred (ice bath 0 - 5 °C). Triethylamine (1.1 equiv.) was added dropwise (acid scavenger), after which chloroacetyl chloride (1.1 equiv.) was added dropwise while stirring slowly. When complete, the mixture was allowed to reach room temperature and stirred for 6 hours. Progress was monitored by TLC. The mixture was washed with water, dilute hydrochloric acid, and brine. The organic layer that remained was dried over anhydrous sodium sulfate and filtered. The solvent was removed under reduced pressure, and the crude product was purified by recrystallization from ethanol to afford 1-(chloroacetyl) benzotriazole.

1-(1H-benzo[d][1, 2, 3] triazol-1-yl) -2-chloroethan-1-one (a)

^{1}H NMR (400 MHz, DMSO-d_6) δ 8.08-7.22 (m, 4H, Ar-H), 4.85 (s, 2H, -CO-CH_2-); ^{13}C NMR (100 MHz, DMSO-d_6) δ 163.17 (1C, -CO-), 145.03, 132.44, 128.51, 124.06, 119.93, 113.71 (6 C, Aromatic carbons), 47.25 (1C, -CH_2-).

2.2 Synthesis of Benzotriazole Acetohydrazide Derivative (b)

1-(Chloroacetyl) benzotriazole (1 equiv.) was dissolved in DMF, and then hydrazine hydrate (2.5 equiv.) was added dropwise with stirring. Heating under reflux for 6 hours, monitored by TLC. Once finished, it was cooled to room temperature and poured into cold water (precipitate). Filtered, washed thoroughly with cold water, and recrystallized from ethanol (yield).

1-(1H-benzo[d][1, 2, 3]triazol-1-yl) -2-hydrazineylethan-1-one (b)

^{1}H NMR (400 MHz, DMSO-d_6) δ 8.21-7.27 (m, 4H, Ar-H),6.47 (s, ^{1}H, -NH),4.67 (s, 2H, -NH2), 4.24 (s, 2H, -CO-CH2-); ^{13}C NMR (100 MHz, DMSO-d_6) δ 164.65 (1C, -CO-), 144.98, 133.17, 128.51, 124.07, 119.88, 113.71 (6 C, Aromatic carbons), 56.42 (1C, -CH2-).

2.3 Synthesis of Benzotriazole Derivatives (bc1-bc5) [38]

Benzotriazole acetohydrazide derivative (1.0 mmol) was dissolved in anhydrous DMF (5–10 mL) under nitrogen atmosphere with stirring at room temperature. Ice bath was used for cooling the reaction mixture to 0 °C. Isocyanate derivative (1.1 mmol), namely 4-(4-isocyanatophenoxy) phenol, 1-isocyanato-4-(4-methoxyphenoxy) benzene, 1-chloro-3-(4-isocyanatophenoxy) benzene, 1-isocyanato-4-(4-(trifluoromethyl) phenoxy) benzene, 1-isocyanto-4-(4-(methoxystyryl) benzene and (E) -1-isocyanato-4-(4-methoxystyryl) benzene (1.1 mmol), was added dropwise with stirring. The reaction mixture was kept at 0 °C (ice bath) for 1 hour, then allowed to warm to room temperature and stirred for 16–20 hours. Monitoring of the reaction was done through TLC. At completion, the reaction mixture was poured into cold water with stirring to get the precipitate or suspension. The product was extracted with ethyl acetate (3 × 20 mL), and the combined organic layers were washed with brine, dried over

anhydrous sodium sulfate, filtered, and concentrated under reduced pressure to provide the crude product, which was purified by column chromatography on silica gel eluted with ethyl acetate/hexane mixtures (v/v 2:8) to give the corresponding new urea derivatives in good yields.

(A)-2-(2-(1H-benzo[d][1, 2, 3]triazol-1-yl) -2-oxoethyl) -N-(4-(4-hydroxyphenoxy) phenyl) hydrazine-1-carboxamide (bc1)

White solid; yield 73%; Mp: 147–149 °C; FTIR (cm^{-1}, υ**)** 3324 (OH), 3285, 3244, 3197 (**N–H**), 1684 (**C=O** amide); ^{1}H NMR (400 MHz, DMSO-d_6) δ 9.11 (s, ^{1}H, Phenolic, -OH), 8.31 (s, ^{1}H, Ph-NH-CO-, Urea NH), 8.14 (s, ^{1}H, -NH–CO–,Urea NH), 7.89 (s, 1H, Benzotriazole-CO-CH_2–NH proton), 7.88-7.12 (m, 12H, Ar-H), 4.29 (s, 2H, -CO-CH_2-); ^{13}C NMR (100 MHz, DMSO-d_6) δ 164.29 (1C, Benzotriazole-CO-CH_2), 156.49 (1C–NH–CO–NH), 154.50, 153.16, 151.02, 144.65, 136.40, 133.52, 128.38, 124.03, 122.35, 121.34, 119.25, 117.02, 116.28, 113.80 (18 C, Aromatic carbons), 53.21 (1C, -CO-CH_2-); MS (m/z) : 417.28 (M^+); Anal. Calcd. for $C_{21}H_{18}N_6O_4$: C, 60.28; H, 4.34; N, 20.09; Found: C, 60.07; H, 4.31; N, 19.97.

(B)-2-(2-(1H-benzo[d][1, 2, 3]triazol-1-yl) -2-oxoethyl) -N-(4-(4-methoxyphenoxy) phenyl) hydrazine-1-carboxamide (bc2)

White solid; yield 78%; Mp: 168–170 °C; FTIR (cm^{-1}, υ**)** 3312, 3268, 3221 (**N–H**), 1671 (**C=O** amide) ; ^{1}H NMR (400 MHz, DMSO-d_6) δ 8.34 (s, 1H, Ph-NH-CO-, Urea NH), 8.19 (s, 1H, -NH–CO–, Urea NH), 7.95 (s, 1H, Benzotriazole-CO-CH_2–NH proton), 7.85-7.08 (m, 12H, Ar-H), 4.31 (s, 2H, -CO-CH_2-), 3.84 (s, 3H, -OCH_3); ^{13}C NMR (100 MHz, DMSO-d_6) δ 165.11 (1C, Benzotriazole-CO-CH_2), 156.87 (1C–NH–CO–NH), 154.87, 153.01, 150.45, 144.35, 136.48, 133.87, 128.87, 124.78, 122.57, 121.49, 119.47, 117.27, 116.47, 113.24 (18 C, Aromatic carbons), 55.57 (1C, -O-CH_3), 53.35 (1C, -CO-CH_2-); MS (m/z) : 432.22 (M^+); Anal. Calcd. for $C_{22}H_{20}N_6O_4$: C, 61.10; H, 4.66; N, 19.43; Found: C, 60.98; H, 4.63; N, 19.31.

(C)-2-(2-(1H-benzo[d][1, 2, 3]triazol-1-yl) -2-oxoethyl) -N-(4-(3-chlorophenoxy) phenyl) hydrazine-1-carboxamide (bc3)

White solid; yield 69%; Mp: 174–176 °C; FTIR (cm^{-1}, υ) 3302, 3274, 3212 (**N–H**), 1665 (**C=O** amide) ; 1H NMR (400 MHz, DMSO-d_6) δ 8.28 (s, 1H, Ph-NH-CO-, Urea NH), 8.17 (s, 1H, -NH–CO–,Urea NH), 7.91 (s, 1H, Benzotriazole-CO-CH2–NH proton), 7.82-7.02 (m, 12H, Ar-H), 4.33 (s, 2H, -CO-CH2-); ^{13}C NMR (100 MHz, DMSO-d_6) δ 165.88 (1C, Benzotriazole-CO-CH2), 157.92 (1C–NH–CO–NH), 155.49, 152.78, 144.66, 136.40, 134.18, 133.52, 130.36, 128.38, 124.54, 123.99, 121.41, 120.89, 120.06, 119.60, 117.01, 113.79 (18 C, Aromatic carbons), 53.14 (1C, -CO-CH2-); MS (m/z) : 435.56 (M^+); Anal. Calcd. for $C_{21}H_{17}ClN_6O_3$: C, 57.74; H, 3.92; N, 19.24; Found: C, 57.32; H, 3.93; N, 19.15.

(D)-2-(2-(1H-benzo[d][1, 2, 3]triazol-1-yl) -2-oxoethyl) -N-(4-(4-(trifluoromethyl) phenoxy) phenyl) hydrazine-1-carboxamide (bc4)

White solid; yield 74%; Mp: 195–197 °C; FTIR (cm^{-1}, υ) 3289, 3271, 3223 (N–H), 1659 (C=O amide) ; 1H NMR (400 MHz, DMSO-d_6) δ 8.32 (s, 1H, Ph-NH-CO-, Urea NH), 8.19 (s, 1H, -NH–CO–,Urea NH), 7.89 (s, 1H, Benzotriazole-CO-CH2–NH proton), 7.89-7.11 (m, 12H, Ar-H), 4.31 (s, 2H, -CO-CH2-); ^{13}C NMR (100 MHz, DMSO-d_6) δ 167.12 (1C, Benzotriazole-CO-CH2), 158.74 (1C–NH–CO–NH), 154.75, 153.08, 144.52, 136.57, 134.86, 133.21, 130.78, 128.85, 123.56, 122.66, 120.96, 120.14, 119.54, 117.23, 113.18 (18 C, Aromatic carbons),

124.89 (1C, -CF3), 53.27 (1C, -CO- CH2-); MS (m/z) : 468.97 (M^+); Anal. Calcd. for $C_{22}H_{17}F_3N_6O_3$: C, 56.17; H, 3.64; N, 17.87; Found: C, 56.01; H, 3.61; N, 17.73.

(E) -2-(2-(1H-benzo[d][1, 2, 3]triazol-1-yl) -2-oxoethyl) -N-(4-(4-methoxystyryl) phenyl) hydrazine-1-carboxamide (bc5) :

White solid; yield 70%; Mp: 209–211°C; FTIR (cm^{-1}, υ) 3311, 3284, 3179 (**N–H**), 1669 (**C=O** amide) ; 1H NMR (400 MHz, DMSO-d_6) δ 8.36 (s, 1H, Ph-NH-CO-, Urea NH), 8.24 (s, 1H, -NH–CO–,Urea NH), 7.86 (s, 1H, Benzotriazole-CO-CH2–NH proton), 7.92-7.14 (m, 12H, Ar-H),6.92 (d, J = 15.4 Hz, 1H, vinyl Ha, Urea–Ph–CH=), 6.63 (d, J = 15.1 Hz, 1H, vinyl Hb, =CH–Ph-OCH_3), 4.34 (s, 2H, -CO-CH2-), 3.82 (s, 3H, OCH_3); ^{13}C NMR (100 MHz, DMSO-d_6) δ 166.54 (1C, Benzotriazole-CO-CH2), 158.14 (1C–NH–CO–NH), 156.22, 144.51, 140.65, 133.42, 131.97, 130.21, 127.42, 126.44, 124.12, 121.29, 119.61, 115.24, 113.27 (18 C, Aromatic carbons), 129.12, 127.57 (2C, Vinyl-CH=CH-), 56.19 (1C, -O-CH3), 53.28 (1C, -CO-CH2-); MS (m/z) : 441.81 (M^+); Anal. Calcd. for $C_{24}H_{22}N_6O_3$: C, 65.15; H, 5.01; N, 18.99; Found: C, 64.89; H, 5.03; N, 18.91.

2.4 Molecular Docking studies

Molecular Operating Environment (MOE) software was used to predict the binding affinity of synthesized urea–benzotriazole derivatives (bc1-bc5) against VEGFR-2 (PDB ID: 4ASD). VEGFR-2 3D structure [38]. The 3D crystal structure of VEGFR-2 was retrieved from the protein data bank and processed by deleting all water molecules and co-crystallized ligands, and subsequent protonation and energy minimization were performed with the default Amber99 force field. All water molecules, except for H-O-H2142 and H-O-H2205, were pruned during protein preparation, and crystal ligand water molecules were intact. Ligands were drawn in MOE and energy minimized with the MMFF94x force field. Docking was carried out with the ligand that was co-crystallized to characterize the active site to which docking was directed (placement methodology "Triangle Matcher" and refinement method applied was 'Rigid Receptor'). Binding scores were sorted by the London dG score function. Docking data suggested that all the compounds formed stable complexes involving the key active site residues Glu885, Asp1046 and Cys919, with AS4 and AS5 having the highest affinities of binding, presumably via halogen bond contacts and hydrophobic interactions. Such interactions between the model and the VEGFR-2 suggests a potential strong inhibitory activity against VEGFR-2 and supports them as potential anticancer agents.

4. Results and discussion

Construction of the target benzotriazole-based urea derivative proceeded stepwise starting with N1-acylation of benzotriazole using chloroacetyl chloride in the presence of triethylamine to afford 1-(chloroacetyl) benzotriazole (a) Figure 1. The formation of this molecule was confirmed by the appearance of the characteristic carbonyl signal in the ^{1}H NMR spectrum at around δ 163 ppm and a methylene singlet around δ 4.85 ppm in the 1H NMR spectrum. Nucleophilic substitution with hydrazine hydrate gave the corresponding acetohydrazide (b), this transformation being evidenced by the appearance of both the hydrazide NH and NH2 signals in the ^{1}H NMR spectrum and a downfield methylene carbon signal (from the methyl acetyl moiety), thus confirming the displacement of Cl by the hydrazine moiety. The hydrazide intermediate finally reacted with a variety of substituted aromatic isocyanates (bc1–bc5) in an anhydrous DMF solvent under nitrogen to furnish a new series of urea derivatives that were obtained in good yields (69–78%). The structures were confirmed from FTIR absorption bands due to N–H and

amide carbonyl groups, ^{1}H NMR singlets for the two urea NH protons, aromatics multiplets consistent with the benzotriazole and substituted phenyl rings, and methylene signals at about δ 4.3 ppm. In addition, substituent-specific signals, such as phenolic OH, methoxy, trifluoromethyl, chloro, and trans-vinyl protons were consistent with the proposed structures and the ^{13}C NMR spectra showed two carbonyl carbons from an amide and from urea. The presence of the molecular ion peaks in the mass spectra and the close agreement between calculated and found values for elemental analysis evidenced the molecular formulas and high purity of the synthesised compounds and confirmed the successful preparation of a structurally diverse library of benzotriazole-linked urea derivatives for further biological investigation.

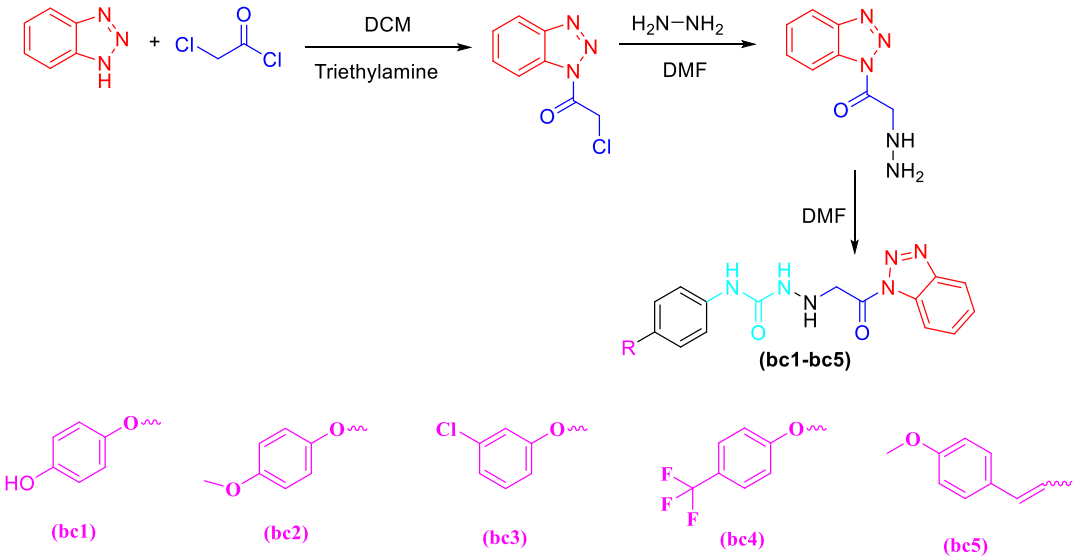

Figure 1: Synthesis of the target benzotriazole-based urea derivatives (bc1-bc5)

4.1 Validation of the Molecular Docking Protocol

The reliability of the molecular docking protocol was validated through a re-docking procedure of the native co-crystallized ligand into the catalytic binding site of VEGFR-2 [38, 39]. In this case, the native ligand was removed from the crystal structure and then redocked under identical conditions used for our designed compounds. As shown in Figure 2, the super-imposition between the re-docked pose (pink) and the native as observed crystallographically (green) displays a high degree of overlap in the VEGFR-2 active site. The close agreement of both conformations suggests that the docking methodology accurately reproduced the experimentally determined binding mode. The preservation of key interactions in the catalytic pocket is further testament to the robustness of our procedure. Our re-docked ligand makes the same key hydrogen bonding interactions with critical amino acid residues, such as Cys919 and Asp1046, important in kinase inhibition. Moreover, an optimal pose was indicated by hydrophobic contacts with surrounding residues in particular, Phe1047, Ile1044, Leu840, and Val848 what strengthen the orientation of the ligand in the ATP-binding pocket. The similarity of these interactions to the contacts seen in the crystallographic structure also suggests that our docking settings, grid parameters, and scoring function are properly optimized. In conclusion, the strong spatial superimposition and retention of critical intermolecular forces confirms the validity and predictive accuracy of our method. Thus, the validated model was

used for subsequent docking studies and binding affinity predictions of the newly synthesized benzotriazole-based urea derivatives against VEGFR-2.

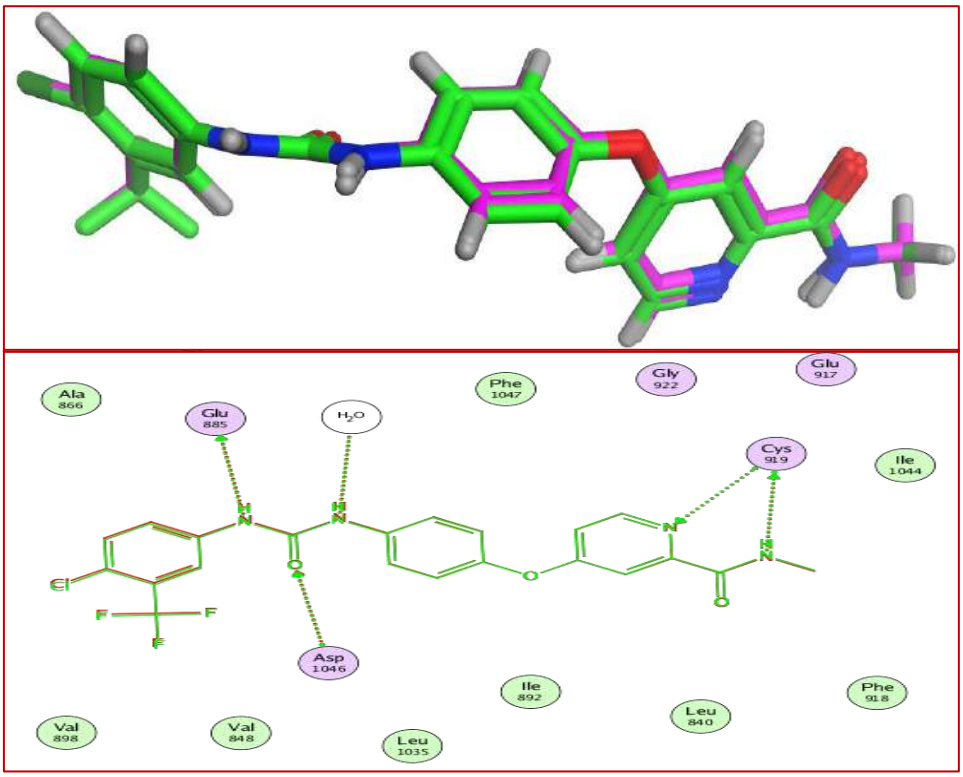

Figure 2: The native ligand (green) and the resulting posture (red) are the outcomes of the re-docking procedure into the VEGFR-2 catalytic site.

4.2 Molecular Docking Studies

Molecular docking was performed to evaluate the binding affinity and interaction profile of the synthesized benzotriazole-based urea derivatives (bc1–bc5) toward the VEGFR-2 kinase domain (PDB ID: 4ASD), using Sorafenib as the reference inhibitor. The docking scores Table 1 indicate that all the synthesized compounds exhibited favorable binding energies within the ATP-binding pocket, ranging from -8.77 to -9.37 kcal/mol, compared with Sorafenib (-9.85 kcal/mol). These results suggest strong and competitive binding interactions with the target enzyme. Among the tested compounds, bc2 showed the best docking score (-9.37 kcal/mol), followed by bc5 (-9.04 kcal/mol) and bc4 (-8.96 kcal/mol), indicating enhanced affinity toward VEGFR-2. The improved binding of bc2 may be attributed to the presence of the trifluoromethyl-substituted phenoxy group, which enhances hydrophobic interactions and stabilizes the ligand within the binding cavity. Likewise, bc5 formed multiple hydrogen bonds and had a larger π-conjugation that may allow better fitting in the hydrophobic pocket Figure 3-Figure 7. The investigation of the interaction patterns showed that hydrogen bonding notably contributed to predicting ligand–protein complexes. Some of the main amino acids involved were CYS919, ASP1046, GLU885, and CYS917, which are all well known catalytic and hinge region residues implicated in VEGFR-2 inhibition.

Com.	Amino acid	Distance (A)	E (kcal/mol)	Interaction type	Mol Dock Score	Rmsd
bc1	GLU 885	2.95	-1.0	H-donor	-8.7689	1.7824
	HOH 2142	2.99	-1.9	H-donor		
	HOH 2142	3.28	-0.6	H-donor		
	CYS 919	3.05	-0.8	H-donor		
	ASP 1046	2.90	-2.9	H-acceptor		
	LEU 840	4.07	-0.7	pi-H		
	ASP 1046	3.71	-1.2	pi-H		
bc2	GLU 885	2.79	-4.9	H-donor	-9.3684	1.6301
	HOH 2142	2.99	-1.9	H-donor		
	ASP 1046	2.90	-2.9	H-acceptor		
	LEU 840	3.94	-0.6	pi-H		
bc3	ASP 1046	2.96	-2.6	H-donor	-8.8338	1.8547
	LEU 840	4.11	-0.6	pi-H		
	CYS 1045	3.88	-1.1	pi-H		
bc4	HOH 2142	2.92	-0.4	H-donor	-8.9577	1.7339
	ASP 1046	3.15	-2.8	H-acceptor		
	LEU 840	4.03	-0.6	pi-H		
bc5	GLU 885	3.08	-3.3	H-donor	-9.0379	1.0414
	HOH 2142	2.97	-1.4	H-donor		
	ASP 1046	2.87	-1.9	H-acceptor		
	LEU 840	4.33	-0.8	pi-H		
	LEU 840	3.88	-0.9	pi-H		
	ASP 1046	3.52	-0.7	pi-H		
Sorafenib	CYS 919	2.94	-0.8	H-donor	-9.8547	1.3244
	HOH 2142	2.93	-2.8	H-donor		
	GLU 885	2.98 3.22 2.21	-3.7	H-donor		
	CYS 917		-2.4	H-acceptor		
	ASP 1046		-2.0	H-acceptor		

Table 1: The molecular docking scores and binding interaction of ligands (bc1- bc5) and Sorafenib against 4ASD

Notably, several of them formed hydrogen bond interactions with ASP1046, a residue crucial for the activation loop, indicating good anchorage within the kinase domain. Additionally, interactions with CYS919 (present in the hinge region) allow us to say that the orientation of the ligands in the ATP-binding site is likely correct, and consistent with known VEGFR-2-inhibitors. We have strong indications of the presence of critical hydrophobic and π–H interactions with LEU840, CYS1045, and with surrounding hydrophobic residues, indicating that these compounds are anchored in a stable fashion. These non-covalent interactions serve to support the aromatic systems of synthesized compounds inside the hydrophobic pocket to favorably stabilize the binding of the entire molecule and were crucial to enhance the binding affinity of the synthesized derivatives. The RMSD values (1.04–1.85 Å) confirm that all the docked conformations are within limits (<2.0 Å). The fact that the general mode of binding was in a similar fashion for the entire series of these compound derivatives confirms their suitability of binding to VEGFR-2 with the benzotriazol–urea scaffold. Overall lessons gleaned from results of docking ensured us that each of the synthesized derivatives possessed strong binding affinity toward VEGFR-2, and an estimated degree of anti-cancer activity strength would be similar to that observed for the reference drug, Sorafenib. The presence of electron-withdrawing groups (CF_3, Cl) and extended aromatic systems seems to promote binding on the basis of hydrogen bond and hydrophobic interactions. Overall, these results suggest that the designed compounds are suitable VEGFR-2 inhibitors and deserve further biological evaluation and SAR studies.

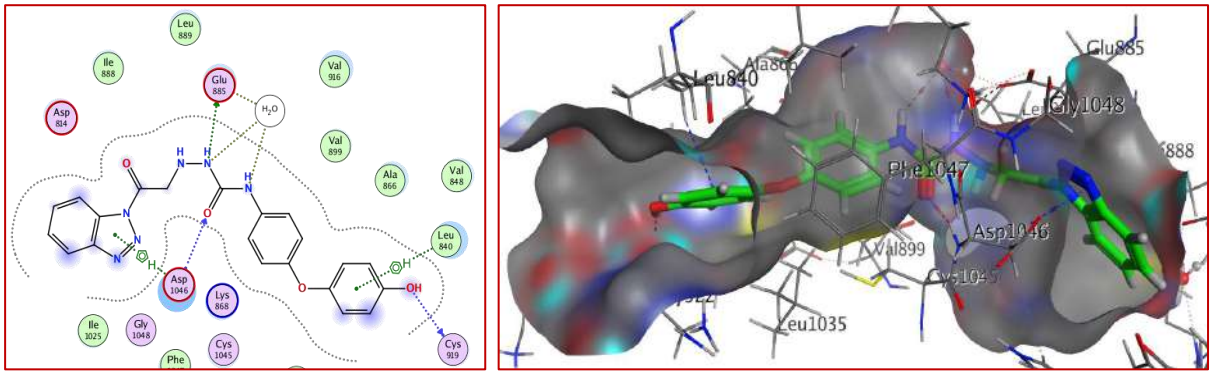

Figure 3: 3-D and 2-D interactions between bc1docked with 4ASD active residues and type of interaction

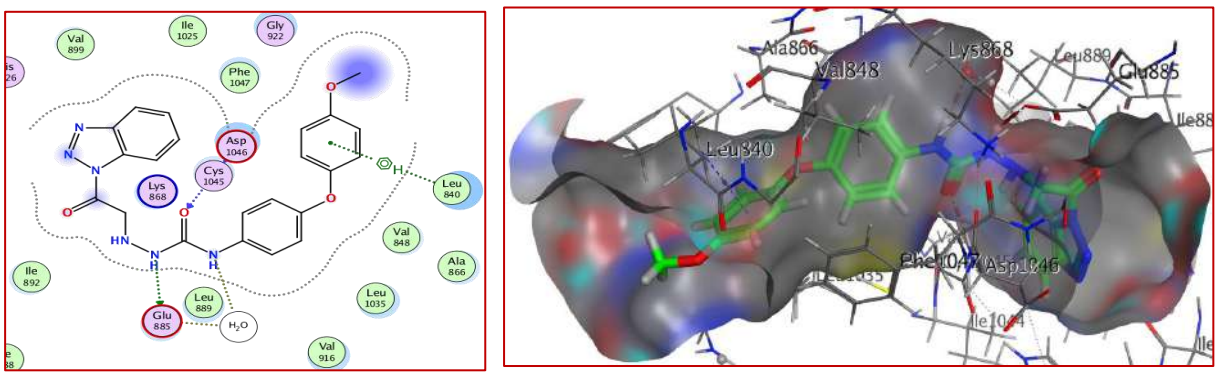

Figure 4: 3-D and 2-D interactions between bc2 docked with 4ASD active residues and type of interaction

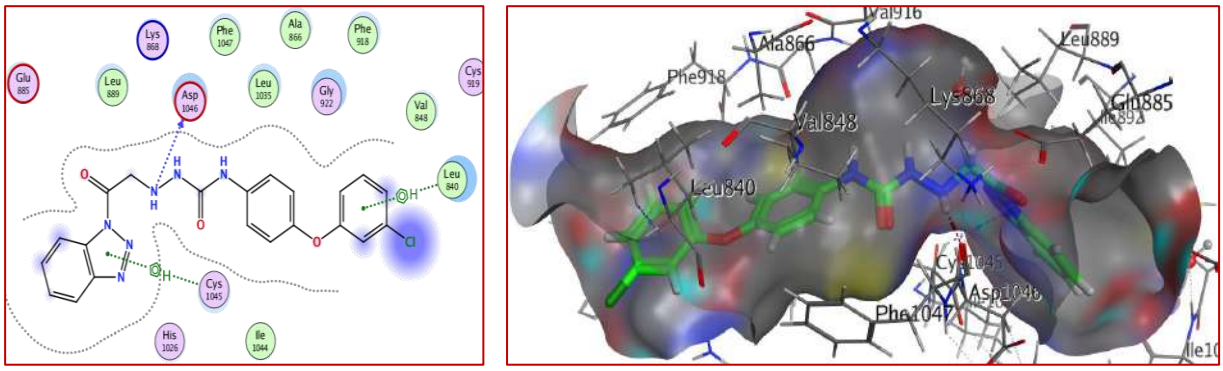

Figure 5: 3-D and 2-D interactions between bc3 docked with 4ASD active residues and type of interaction

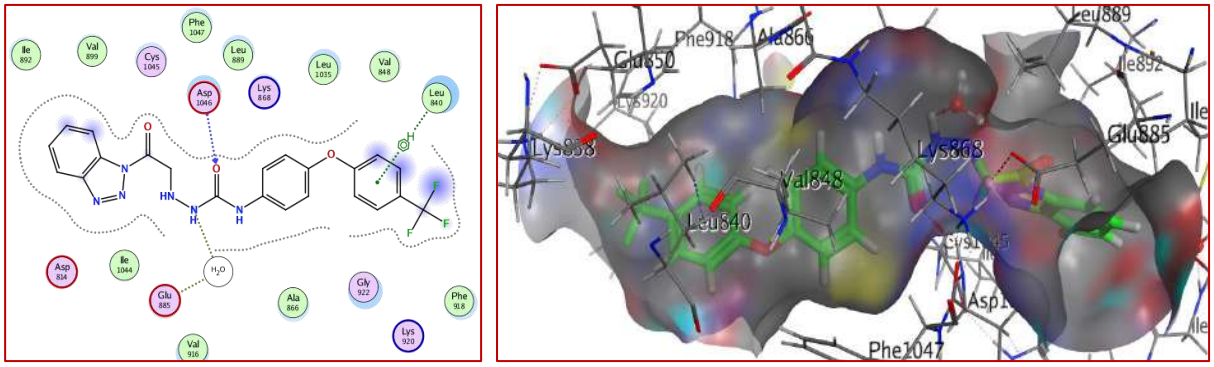

Figure 6: 3-D and 2-D interactions between bc4 docked with 4ASD active residues and type of interaction

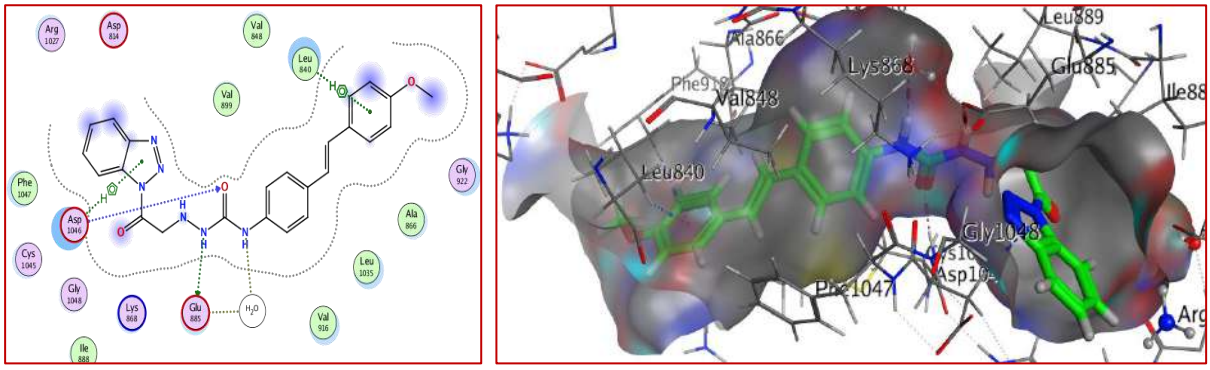

Figure 7: 3-D and 2-D interactions between bc5 docked with 4ASD active residues and type of interaction

4.3 Structure Activity Relationship (SAR) Study

The structure activity relationship (SAR) for the synthesized benzotriazole-based urea derivatives (bc1–bc5) was built on the molecular docking scores and interactions in the active site of VEGFR-2 (PDB ID: 4ASD). The designed compounds shared a common pharmacophoric skeleton comprising three indispensable structural moieties: (i) a benzotriazole nucleus, (ii) a hydrazide–urea linker, and (iii) a substituted phenoxy/aryl moiety.

Modifications were primarily introduced towards the terminal aromatic region to investigate the influence of various substituents on binding affinity and interaction profile. The benzotriazole scaffold is postulated to serve as an anchoring moiety within the ATP-binding pocket. In all derivatives, this ring system was involved in π–π and hydrophobic interactions with residue lining the binding cavity. The adjacent carbonyl group increased potential hydrogen-bonding capacity with residues in the hinge-region such as CYS919 and ASP1046 important for kinase inhibition, thus confirming that the benzotriazole nucleus is an obligatory structural element for activity. The hydrazide–urea moiety is crucial for activity as an H-bond donor/acceptor system: all active compounds formed at least one or two H-bonds with GLU885, CYS919, and ASP1046. The presence of 2 NH groups in the urea function allowed for multiple stabilising interactions, mimicking the binding mode of known VEGFR-2 inhibitors like Sorafenib: for effective VEGFR-2 binding, the urea pharmacophore is therefore essential. The biological activity was predominantly based on the electronic nature and steric nature of the substituents of the terminal phenyl/phenoxy ring: Electron-withdrawing groups (CF_3, Cl) increased binding affinity. For instance, bc2 (with a trifluoromethyl group) exhibited the best docking score among the synthesized compounds, possibly due to enhanced hydrophobic contacts and a better fit into the lipophilic pocket of VEGFR-2. Electron-withdrawing groups may also increase the electrophilicity of the urea carbonyl, which can enhance hydrogen bonding interactions. Methoxy substitution (electron-donating group), as in bc3 and bc5, provided moderate to strong activity. The methoxy group can enhance π-electron density and lead to some additional van der Waals interactions, although the electron dealing interaction might slightly decrease the hydrogen bonding strength compared to strongly with drawing groups. A styryl extension (bc5) improved activity through enhanced molecular planarity and π-conjugation leading to increased hydrophobic and π–π stacking interactions in the binding pocket. The trans-configuration (as suggested by the large coupling constants observed in NMR) likely aids in orienting the molecule appropriately within the active site. The introduction of a hydroxyl (bc1) enabled further additional hydrogen bonding but is a somewhat less potent binder than CF_3-containing derivatives; the increased polarity and penalties associated with partial desolvation within the hydrophobic pocket may play a role.

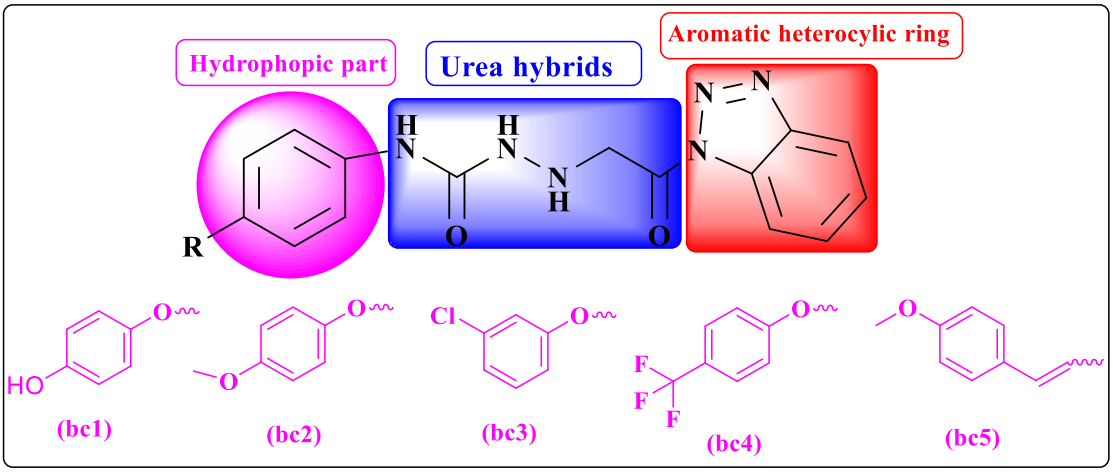

Figure 8: Model chemical structure of prepared compounds bc1-bc5 as known VEGFR-2 inhibitors.

According to the SAR analysis optimal activity requires a balance between equatorial hydrogen bonding interactions (via the urea and amide functionalities) and the hydrophobic contacts of substituted aromatic rings. Compounds with strong hydrogen bond donors/acceptors supplemented by lipophilic substituents had higher

docking scores. Our results led us to conclude that the benzotriazole–urea framework constitutes a basic structural feature of active VEGFR-2 inhibitors. Part of the binding affinity is accounted for by strong hydrogen bonds to hinge and activation loop residues in the following order CYS919, ASP1046, and GLU885 being key players. The presence of electron-withdrawing groups on the terminal aromatic ring greatly increases the biological activity, likely because of better hydrophobic interactions, as well as a better fit into the active site. Extending the aromatic system provides stronger hydrophobic stabilization that lies inside the ATP-binding pocket. Collectively, these findings imply that future structural optimizations should target the introduction of more lipophilic electron-withdrawing substituents while retaining the urea pharmacophore to further enhance VEGFR-2 inhibitory activity.

5. ADMET Properties

The predicted ADMET profile for the synthesized benzotriazole-based urea derivatives (bc1–bc5) suggests generally favorable pharmacokinetic characteristics with some concerns regarding safety Table 2. With regard to absorption, the compounds have been predicted to have moderate water solubility values (log S = -3.82 to -4.60), which indicates favorable, but limited aqueous solubility consistent with moderately lipophilic kinase inhibitors. The predicted Caco-2 permeability values of 0.588–0.845 log Papp and high predicted human intestinal absorption (79–85%) is also consistent with the compounds having good oral bioavailability potential, with bc5 demonstrating the highest permeability. The skin permeability values (log Kp ≈ −2.73) suggest low dermal absorption, which is favorable for orally administered agents. All of the derivatives are predicted to be P-glycoprotein substrates, which will influence their efflux and therefore bioavailability. Importantly, however, most of the compounds (excluding bc1) are predicted P-gp I inhibitors, which could reduce efflux-related resistance via these mechanisms. The distribution of these compounds is suggested by the prediction of VDss values (−0.37 to −0.55 log L/kg) indicating them to be moderately distributed within body tissues. Low fraction unbound (Fu = 0.01–0.06) indicates high plasma protein binding, a feature frequently seen in lipophilic, aromatic compounds. BBB permeation values (log BB ≈ −1.5 to −1.96) and CNS permeation (log PS ≈ −2.3 to −3.2) suggest a poor CNS penetration, which may aid by ensuring central nervous system-related side effects are minimised in anticancer therapy. In metabolism, predicting that none of the compounds are CYP2D6 substrates whilst all are CYP3A4, indicates hepatic metabolism is likely via CYP3A4. All derivatives indicating inhibitory potential against CYP1A2, CYP2C19, CYP2C9 and CYP3A4 points toward possible drug–drug interaction risks which ought to be considered in further development. In excretion, total clearance values that differ only modestly in (−0.246 to 0.178 log ml/min/kg) are suggestive of not particularly fast clearance and of note, none of the compounds being predicted to be renal OCT2 substrates indicates renal transporter-mediated excretion is also less likely. To assess the toxicity profile: all are AMES predicted positives and potentially hepatotoxic; indicating mutagenicity/liver toxicity issues that will need experimental validation. None are predicted hERG I inhibitors, with a resultant lower risk of severe cardiotoxicity, but all are predicted hERG II inhibitors, requiring further cardiac safety evaluation. The predicted oral rat acute toxicity (LD50 = 2.48–2.88 mol/kg) suggests moderate toxicity, and the chronic toxicity (LOAEL values, etc.) varies but is acceptable in terms of experimental work. No skin sensitization predicted. From a physicochemical perspective: molecular weights in the indicated range (418–470 Da), LogP (2.89–4.21), hydrogen bond donors (3–4), acceptors (7–8), rotatable bonds (6–7), surface area values, and are generally Lipinski rule of five compliant; supportive of drug-likeness and oral bioavailability. In summary, the ADMET analysis indicates that the synthesized derivatives have amenable oral absorption, moderate distribution, and suitable physicochemical

profile, though CYP inhibition, mutagenicity and hepatotoxicity should be further explored in future in vitro and in vivo generations of these derivatives to confirm their appropriateness for use.

Property	**Model Name**	**(bc1)**	**(bc2)**	**(bc3)**	**(bc4)**	**(bc5)**	**Unit**
Absorption	Water solubility	-3.828	-4.419	-4.338	-4.396	-4.603	Numeric (log mol/L)
	Caco2 permeability	0.588	0.648	0.603	0.601	0.845	Numeric (log Papp in 10^{-6} cm/s)
	Intestinal absorption (human)	79.732	84.194	83.817	84.892	84.127	Numeric (% Absorbed)
	Skin Permeability	-2.735	-2.736	-2.736	-2.736	-2.736	Numeric (log Kp)
	P-glycoprotein substrate	Yes	Yes	Yes	Yes	Yes	Categorical (Yes/No)
	P-glycoprotein I inhibitor	No	Yes	Yes	Yes	Yes	Categorical (Yes/No)
	P-glycoprotein II inhibitor	Yes	Yes	Yes	Yes	Yes	Categorical (Yes/No)
Distribution	VDss (human)	-0.372	-0.439	-0.514	-0.55	-0.477	Numeric (log L/kg)
	Fraction unbound (human)	0.061	0.028	0.014	0.01	0.029	Numeric (Fu)
	BBB permeability	-1.858	-1.864	-1.831	-1.968	-1.569	Numeric (log BB)
	CNS permeability	-3.216	-3.186	-2.404	-2.361	-2.558	Numeric (log PS)
Metabolism	CYP2D6 substrate	No	No	No	No	No	Categorical (Yes/No)
	CYP3A4 substrate	Yes	Yes	Yes	Yes	Yes	Categorical (Yes/No)
	CYP1A2 inhibitior	Yes	Yes	Yes	Yes	Yes	Categorical (Yes/No)
	CYP2C19 inhibitior	Yes	Yes	Yes	Yes	Yes	Categorical (Yes/No)
	CYP2C9 inhibitior	Yes	Yes	Yes	Yes	Yes	Categorical (Yes/No)
	CYP2D6 inhibitior	No	No	No	No	No	Categorical (Yes/No)
	CYP3A4 inhibitior	Yes	Yes	Yes	Yes	Yes	Categorical (Yes/No)
Excretion	Total Clearance	0.011	0.073	-0.231	-0.246	0.178	Numeric (log ml/min/kg)
	Renal OCT2 substrate	No	No	No	No	No	Categorical (Yes/No)
Toxicity	AMES toxicity	Yes	Yes	Yes	Yes	Yes	Categorical (Yes/No)
	Max. tolerated dose (human)	0.834	0.791	0.778	0.766	0.68	Numeric (log mg/kg/day)
	hERG I inhibitor	No	No	No	No	No	Categorical (Yes/No)
	hERG II inhibitor	Yes	Yes	Yes	Yes	Yes	Categorical (Yes/No)

	Oral Rat Acute Toxicity (LD50)	2.484	2.814	2.72	2.695	2.879	Numeric (mol/kg)
	Oral Rat Chronic Toxicity (LOAEL)	1.515	1.151	1.332	1.237	1.519	Numeric (log mg/kg_bw/day)
	Hepatotoxicity	Yes	Yes	Yes	Yes	Yes	Categorical (Yes/No)
	Skin Sensitisation	No	No	No	No	No	Categorical (Yes/No)
	T.Pyriformis toxicity	0.288	0.288	0.29	0.289	0.288	Numeric (log ug/L)
	Minnow toxicity	3.233	2.832	2.483	2.566	4.189	Numeric (log mM)
Molecular Weight		418.413	432.44	436.859	470.411	442.479	g/mol
LogP		2.8957	3.1987	3.8435	4.2089	3.5768	
Rotatable Bonds		6	7	6	6	7	
Hydrogen bonds Acceptors		8	8	7	7	7	
Hydrogen bonds Donors		4	3	3	3	3	
Surface Area		175.968	182.652	181.477	190.035	189.579	

Table 2. Physicochemical characteristics and ADMET profile of compounds (bc1-bc5)

6. Conclusions

In the current study, a new series of benzotriazole-derived urea derivatives (bc1–bc5) were designed and synthesized by a simple multi-step synthetic route starting from benzotriazole. The obtained compounds were characterized by FTIR, ^{1}H NMR, ^{13}C NMR, mass spectroscopy, and elemental analysis. Molecular docking studies against the VEGFR-2 kinase domain (PDB ID: 4ASD) demonstrated that all synthesized compounds exhibited favorable binding affinities within the ATP-binding pocket, with docking scores ranging from −8.77 to −9.37 kcal/mol. However, these values were slightly lower than that of the reference inhibitor Sorafenib (−9.85 kcal/mol). Among the synthesized derivatives, bc2 displayed the highest docking score. The compounds engaged in notable hydrogen bond interactions with key residues such as CYS919, ASP1046, and GLU885, as well as stabilizing hydrophobic and π–π interactions. Amongst the series, bc2 exhibited the best docking score, highlighting the beneficial role of electron-withdrawing substituents, such as the trifluoromethyl group. Structure–activity relationship (SAR) analysis established that the benzotriazole–urea scaffold serves as a key pharmacophoric ‘warhead’ for VEGFR-2 inhibition. The structural requirement of hydrogen-bond donors and acceptors within the urea, along with hydrophobic aromatic substitutions, is vital for effective binding within the kinase active site. ADMET prediction indicated that these compounds should have good oral absorption,

acceptable physicochemical properties, and general compliance with Lipinski's rule of five. Predicted CYP450 inhibition, AMES positivity, and possible hepatotoxicity suggest the need for further in vitro and in vivo studies to confirm the safety profile and to assess pharmacological performance. In conclusion, the synthesized benzotriazole-based urea derivatives act as promising lead candidates for the discovery of VEGFR-2 targeted anticancer agents and warrant further biological evaluation and optimization.

Article Information

Acknowledgments: The author sincerely thanks the staff of ARCPMS, University of AlKafeel, for their valuable assistance in conducting the anticancer activity tests and supporting the completion of this study.

Author Contributions: Mohammed Zuheir Hassan – Conceptualization, Methodology, Data curation, Formal analysis, Writing – original draft, Writing – review & editing, Supervision.

Funding / Financial Support: The authors received no external funding.

Conflict of Interest: The authors declare no competing interests.

Ethical Approval: Not available.

Informed Consent: Not available.

Data Availability Statement: Not available.

Clinical Trial Registration: Not available.

Disclaimer (Artificial Intelligence): The author (s) hereby declare that NO generative AI technologies such as Large Language Models (ChatGPT, COPILOT, etc.), and text-to-image generators have been used during writing or editing of manuscripts.

References

[1] F. Bray, J. Ferlay, J. Soerjomataram, et al., Global cancer statistics 2018: GLOBOCAN estimates of incidence and mortality worldwide for 36 cancers in 185 countries, CA A Cancer J. Clin. 68 (2018) 394–424.

[2] A.B. Umar, S.H. Abdullahi, R.B. Patil, et al., Design of some phthalazine molecules as novel VEGFR-2 target inhibitors through 3D-QSAR modeling, molecular docking and dynamic simulation and pharmacokinetics profiling, J. Umm Al Qura Univ. Appl. Sci. (2024), https://doi.org/10.1007/s43994-024-00197-z.

[3] G. Ioele, M. Chieffallo, M.A. Occhiuzzi, M. DeLuca, A. Garofalo, G. Ragno, F. Grande, Anticancer drugs: recent strategies to improve stability profile, pharmacokinetic and pharmacodynamic properties, Molecules 25 (17) (2022) 5436, https://doi.org/10.3390/molecules27175436, 27.

[4] R. Lugano, M. Ramachandran, A. Dimberg, Tumor angiogenesis: causes, consequences, challenges and opportunities, Cell Mol. Life Sci. 77 (2020) 1745–1770, https://doi.org/10.1007/s00018-019-03351-7.

[5] H. Chu, Y. Wang, Therapeutic angiogenesis: controlled delivery of angiogenic factors, Ther. Deliv. 3 (2012) 693–714.

[6] S. Sajib, F.T. Zahra, M.S. Lionakis, et al., Mechanisms of angiogenesis in microbe-regulated inflammatory and neoplastic conditions, Angiogenesis 21 (2018) 1–14.

[7] S. Guo, L.S. Colbert, M. Fuller, et al., Vascular endothelial growth factor receptor-2 in breast cancer, Biochim. Biophys. Acta Rev. Cancer 1806 (2010) 108–121.

[8] S. Takahashi, Vascular endothelial growth factor (VEGF), VEGF receptors and their inhibitors for antiangiogenic tumor therapy, Biol. Pharm. Bull. 34 (2011) 1785–1788.

[9] S.H. Abdullahi, A. Uzairu, G.A. Shallangwa, et al., Structure based design of some novel 3-methylquinoxaline derivatives through molecular docking and pharmacokinetics studies as novel VEGFR-2 inhibitors, Chem. Afr. 5 (2022) 1967–1978, https://doi.org/10.1007/s42250-022-00485-3.

[10] K. Holmes, O.L. Roberts, A.M. Thomas, M.J. Cross, Vascular endothelial growth factor receptor-2: structure, function, intracellular signalling and therapeutic inhibition, Cell. Signal. 19 (2007) 2003–2012.

[11] N.A. Alsaif, A. Elwan, M.M. Alanazi, et al., Design, synthesis and molecular docking of new [1, 2, 4] triazolo[4, 3-a]quinoxaline derivatives as anticancer agents targeting VEGFR-2 kinase, Mol. Divers. 26 (2022) 1915–1932, https://doi.org/10.1007/s11030-021-10303-6.

[12] M. Shibuya, Vascular endothelial growth factor (VEGF) and its receptor (VEGFR) signaling in angiogenesis: a crucial target for anti- and proangiogenic therapies, Genes Cancer 2 (2011) 1097e1105.

[13] A.K. Olsson, A. Dimberg, J. Kreuger, Claesson-Welsh, VEGF receptor signalling-in control of vascular function, Nat. Rev. Mol. Cell Biol. 7 (2006) 359e371.

[14] C.J. Robinson, Stringer, the splice variants of vascular endothelial growth factor (VEGF) and their receptors, J. Cell Sci. 114 (2001) 853e865.

[15] Y. Takahashi, Y. Kitadai, C.D. Bucana, K.R. Cleary, L.M. Ellis, Expression of vascular endothelial growth factor and its receptor, KDR, correlates with vascularity, metastasis, and proliferation of human colon cancer, Cancer Res. 55 (1995) 3964e3968.

[16] R. Roskoski Jr, Vascular endothelial growth factor (VEGF) signaling in tumor progression, Crit. Rev. Oncol. Hematol. 62 (2007) 179-213.

[17] X. Wang, A. M. Bove, G. Simone, & B. Ma, Molecular bases of VEGFR-2-mediated physiological function and pathological role. Front Cell Dev Biol. (2020), 8: 599281.

[18] R.T. Poon, S.T. Fan, J. Wong, Clinical implications of circulating angiogenic factors in cancer patients, J. Clin. Oncol. Off. J. Am. Soc. Clin. Oncol. 19 (2001) 1207-1225.

[19] M. Simons, E. Gordon, Claesson-Welsh, mechanisms and regulation of endothelial VEGF receptor signalling, Nat. Rev. Mol. Cell Biol. 17 (2016) 611.

[20] L. Xi, J.Q. Zhang, Z.C. Liu, J.H. Zhang, J.F. Yan, Y. Jin, Lin Novel 5-anilinoquinazoline-8-nitro derivatives as inhibitors of VEGFR-2 tyrosine kinase: synthesis, biological evaluation and molecular docking, Org. Biomol. Chem. 11 (2013) 4367e4378.

[21] F. Rahim, R. Hussain, S. Subhan, H. Ullah, M.M. Bekhit, M.S. Alnbaheen, A. S. Algarni, S. Aghayeva, Synthesis, in vitro β-glucuronidase inhibition of benzoxazole bearing thiosemicarbazide derivatives along with in silico molecular docking study, Results Chem. 9 (2024) 101635.

[22] M.S. Nadeem, S. Hayat, F. Rahim, J.A. Khan, H. Ullah, S. Iftikhar, K. Muhammad, Synthesis, biological evaluation, molecular docking and dynamic simulation of novel benzofuran derivatives as potential agents against Alzheimer's disease, J. Mol. Struct. 1322 (2025) 140279.

[23] V.S. Anjana, P.M. Kumar, An overview on medicinal perspective and biological behavior of benzotriazole; synthetic study on its multifaceted biological activities, 2025.

[24] T.A. Jimoh, A.O. Oyewale, H. Ibrahim, J.D. Habila, D.E. Arthur, Biological evaluation and docking study of synthesized derivatives of benzotriazole and benzimidazole as antibacterial agents. Chemistry, Africa 5 (3) (2022) 509–523.

[25] A.N. Khayyat, K.O. Mohamed, A.M. Malebari, A. El-Malah, Design, synthesis, and anti-poliferative activities of novel substituted imidazole-thione linked benzotriazole derivatives, Molecules 26 (19) (2021) 5983.

[26] Q. Li, G. Liu, N. Wang, H. Yin, Z. Li, Synthesis and anticancer activity of benzotriazole derivatives, J. Heterocyclic Chem. 57 (3) (2020) 1220–1227.

[27] X. Wang, J. Du, T. Zhou, X. Fang, H. Yang, Novel benzotriazole-benzimidazole metal complexes: structure-activity relationship, synthesis, characterization, and antidiabetic activity, J. Mol. Struct. 1292 (2023) 136141.

[28] R. Ibba, S. Piras, P. Corona, F. Riu, R. Loddo, I. Delogu, G. Collu, G. Sanna, P. Caria, T. Dettori, A. Carta, Front. Chem. 9 (2021) 660424.

[29] G. Semple, P.J. Skinner, M.C. Cherrier, P.J. Webb, C.R. Sage, S.Y. Tamura, R. Chen, J.G. Richman, D.T. Connolly, J. Med. Chem. 49 (2006) 1227.

[30] S.H. Abdullahi, A. Uzairu, G.A. Shallangwa, S. Uba, A.B. Umar, Molecular docking, ADMET and pharmacokinetic properties predictions of some di-aryl pyridinamine derivatives as estrogen receptor (ERþ) kinase inhibitors, Egypt. J. Basic Appl. Sci. 9 (1) (2022) 180–204.

[31] S.H. Abdullahi, A. Uzairu, G.A. Shallangwa, S. Uba, A.B. Umar, In-silico activity prediction, structure-based drug design, molecular docking and pharmacokinetic studies of selected quinazoline derivatives for their antiproliferative activity against triple negative breast cancer (MDA-MB231) cell line, Bull. Natl. Res. Cent. 46 (2022) 2.

[32] E. Kim, J. Yang, S. Park, Factors affecting success of new drug clinical trials, Ther. Innov. Regul. Sci. 57 (2023) 737–750, https://doi.org/10.1007/s43441-023- 00509-1.

[33] T. Abdizadeh, R. Ghodsi, F. Hadizadeh, 3D-QSAR (CoMFA, CoMSIA) and molecular docking studies on histone deacetylase 1 selective inhibitors, Recent Pat. Anti Cancer Drug Discov. 12 (4) (2017) 365–383.

[34] A. Goudzal, A. ElAissouq, H. ElHamdani, E.G. Hadaji, A. Ouammou, M. Bouachrine, 3D-QSAR modeling and molecular docking studies on a series of 2, 4, 5- trisubstituted imidazole derivatives as CK2 inhibitors, J. Biomol. Struct. Dyn. (2022) 1–15.

[35] F.A. Ugbe, G.A. Shallangwa, A. Uzairu, I. Abdulkadir, Activity modeling, molecular docking and pharmacokinetic studies of some boron-pleuromutilins as anti- wolbachia agents with potential for treatment of filarial diseases, Chem. Data Collect. 36 (2021) 100783.

[36] X. Liu, X. Chen, L. Zhang, P. Zhan, X. Liu, 3D-QSAR and docking studies on piperidine substituted diarylpyrimidine analogues as HIV-1 reverse transcriptase inhibitors, Med. Chem. Res. 24 (8) (2015) 3314–3326.

[37] S. Anusuya, D. Velmurugan, M.M. Gromiha, Identification of dengue viral RNAdependent RNA polymerase inhibitor using computational fragment-based approaches and molecular dynamics study, J. Biomol. Struct. Dyn. 34 (7) (2016) 1512–1532.

[38] H. G. Chfat, A. W. Radhi, A. J. Radhi, and I. Alrubaie, “Design, synthesis, In Silico and in vitro studies urea derivatives as VEGFR-2 inhibitors, ” J Mol Struct, vol. 1343, p. 142863, Oct. 2025, doi: 10.1016/j.molstruc.2025.142863.

[39] Radhi, A. J., Fahad, M. M., Alrubaie, I., Shafiq, N., & Afzal, K. (2025). In silico and in vitro studies of gemcitabine derivatives as anticancer agents. Pharmacia, 72, 1-16.